

## Article

# Enhancing Structural Capacity Assessment with a Novel Failure Decision Function for Rectangular Reinforced Concrete Columns

Petros Christou <sup>1,\*</sup> , Marios Charalambides <sup>2</sup>, Demetris Nicolaides <sup>1</sup>  and Georgios Xekalakis <sup>3</sup> <sup>1</sup> Department of Civil Engineering, Frederick University, Nicosia 1036, Cyprus; d.nicolaides@frederick.ac.cy<sup>2</sup> Department of Business Administration, Center of Sciences, Frederick University, Nicosia 1036, Cyprus; bus.chm@frederick.ac.cy<sup>3</sup> Frederick Research Center, Nicosia 1036, Cyprus; g.xekalakis@frederick.ac.cy

\* Correspondence: p.christou@frederick.ac.cy

**Abstract:** This study introduces the Failure Decision Function, a novel approach for evaluating the structural capacity of rectangular reinforced concrete columns under axial forces and moments, both uniaxial and biaxial. The method simplifies existing practices, enhancing accuracy and integration into design software. The methodology hinges on deriving exact biaxial bending failure surfaces, utilizing integral expressions based on material properties and cross-sectional geometry. This direct integration process uncovers failure surface characteristics previously undocumented. Results confirm the utility of the Failure Decision Function through comparative analysis with established literature, showcasing its potential for simplifying and improving structural capacity assessments. The analytic procedure developed enables efficient computation of failure surfaces, streamlining the inclusion of these functions in structural engineering software in two key ways: (1) compiling a library of pre-calculated functions for quick capacity checks and (2) creating a dynamic application that generates these functions based on specific design parameters, allowing users to explore various load and moment scenarios. In conclusion, the Failure Decision Function represents a significant advancement in structural engineering design, offering an accurate and user-friendly method for assessing column performance under critical loading conditions.

**Keywords:** failure decision function; capacity assessment; design of concrete columns; interaction diagrams; stress integration; biaxial bending; failure surfaces



**Citation:** Christou, P.; Charalambides, M.; Nicolaides, D.; Xekalakis, G. Enhancing Structural Capacity Assessment with a Novel Failure Decision Function for Rectangular Reinforced Concrete Columns. *Inventions* **2024**, *9*, 63. <https://doi.org/10.3390/inventions9030063>

Academic Editors: Katarzyna Antosz, Jose Machado, Erika Ottaviano, Pierluigi Rea, Camelia Claudia Avram and Vijaya Kumar Manupati

Received: 12 April 2024

Revised: 24 May 2024

Accepted: 27 May 2024

Published: 29 May 2024



**Copyright:** © 2024 by the authors. Licensee MDPI, Basel, Switzerland. This article is an open access article distributed under the terms and conditions of the Creative Commons Attribution (CC BY) license (<https://creativecommons.org/licenses/by/4.0/>).

## 1. Introduction

In structural engineering, assessing the capacity of columns is vital to ensure the safety and efficiency of buildings and infrastructure. Traditional methods for analyzing and designing reinforced concrete columns use practical tools like interaction diagrams, which illustrate failure envelopes under axial load and uniaxial or biaxial bending (P-M-M). These diagrams are based on the constitutive relationships of concrete and steel (stress vs. strain), the geometry of the cross-section, and the consideration of the stress vs. strain plane's inclination and orientation, representing various failure modes. The calculation of a point on the envelope corresponds to an inclination and orientation of the neutral axis in the deformed state of the cross-section and the estimation of the axial force and bending moment capacity of the section based on equilibrium and compatibility conditions.

The initial work on interaction diagrams, specifically biaxial design charts for rectangular reinforced concrete sections, was conducted by Grasser and Linse in 1972 [1,2]. Since then, various methods, including manual, experimental, numerical, and analytical approaches, have been developed. Notable contributions by Nilson and Winter, 1991, [3] expanded interaction diagrams to include biaxial bending through three-dimensional failure surfaces. Engineers typically use interaction diagrams in line with code provisions, such as Eurocode 2-clause 5.8.9, although, according to Papanikolaou and Sextos, 2016, [4],

the application of uniform interaction diagrams across Eurocode-compliant countries is not easy due to the variability in specific parameters (e.g., the range of values of the reducing factor for long-term effects in the National Annexes). Another contribution to the state of the art is provided by Bhargav et al., 2023 [5], who introduce an algorithm using a modified thick layer integration approach and a nested bisection method to generate exact load contours and complete interaction surfaces.

Various interaction diagrams describing column behavior resulting from experimental work have been provided by Dundar et al., 2008 [6] and Pallarés et al., 2008 [7]. Further, structural analysis and design software packages use numerical techniques, as presented by Fafitis, 2001 [8], Papanikolaou, 2012 [9], and Matuszak and P. Pluciński, 2014 [10], to produce these diagrams. The fiber method, which involves discretizing the section into smaller elements (fibers) and using the uniaxial stress–strain relationship of each element, was implemented by Lejano, 2007 [11] and further utilized by Christou et al., 2013 [12] and Kwak and Kwak, 2010 [13] to calculate average forces in a section by aggregating the resisting forces of all fibers. In addition, Bouzid and Demagh, 2011 [14] proposed a simple formula to estimate the resistance capacity of biaxially loaded short reinforced concrete columns, facilitating the development of interaction diagrams.

The analytical computation of these diagrams can be complex. Di Laora et al., 2019 [15] introduced an analytical, code-compatible procedure for reinforced concrete circular sections, approximating an analytical solution to the computation of the interaction diagrams without iterations and numerical computation. Rodriguez and Aristizabal-Ochoa, 1999 [16] and Quaranta, Trentadue, and Marano, 2017 [17] addressed this by subdividing the section and employing exact analytical stress distribution for closed-form integration of the resulting expressions. Vaz Rodrigues, 2015 [18] developed an algorithm that subdivides sections into trapezoidal elements using polygon clipping techniques, with exact numerical integration on each trapezoid using the change of variables theorem and Gauss–Legendre integration, 2021 [19]. Additionally, da Silva et al., 2009 [20] demonstrated that closed-form solutions for multi-rectangular sections not only simplify calculations but also enhance computational efficiency. These advancements highlight the diversity and potential precision of techniques available for the structural analysis of reinforced concrete sections.

This study introduces a novel analytical framework for assessing the capacity of short reinforced concrete rectangular columns through the development of a Failure Decision Function (FDF). The underlying theory addresses the mathematical challenge of determining whether a point in space lies inside, on the boundary, or outside a closed three-dimensional surface, such as an ellipsoid, as proposed by Schneider and Eberly, 2002 [21]. This innovative approach simplifies the generation of precise failure surfaces and enhances the practical application of these findings in relevant software and decision-making strategies, potentially reducing computational effort. The findings reveal unique characteristics of the failure surfaces, distinct from those documented in existing literature, offering new insights into the structural behavior of columns. This work underscores the importance of continuous innovation in structural analysis and design, promising significant implications for both theoretical research and practical engineering applications.

## 2. Methods

### 2.1. Model Description and Computational Methodology

Bending in columns arises when an eccentric load, aligned parallel to the vertical axis of the column section, is applied. This eccentricity, denoted as  $e$ , is the distance from the applied load to the column's plastic centroid (PC), as illustrated in Figure 1. This relationship establishes a specific pairing of axial load and bending moment for any given eccentricity, leading to a strain distribution across the column section that can be described by a plane equation. This distribution's interface with the column's cross-sectional plane is marked by a straight line known as the neutral axis (NA) (Figure 2). At the point of failure, this strain distribution corresponds to distinct values of axial load ( $P_T$ ) and bending moments ( $M_{XT}$  and  $M_{YT}$ ), where  $T$  signifies the total values. The resulting interaction

diagrams (for uniaxial bending) and failure surfaces (for biaxial bending) serve as graphical representations of the column's failure across an entire range of eccentricities, as shown in Figure 3.

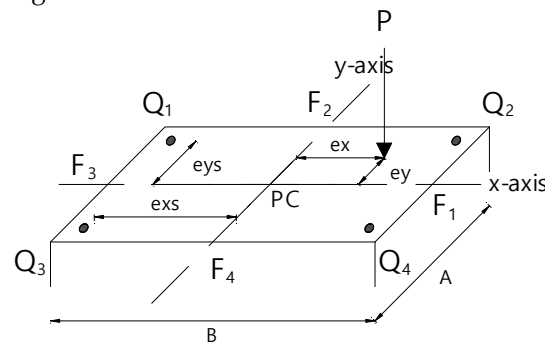


**Figure 1.** Eccentric load applied on an RC column section.

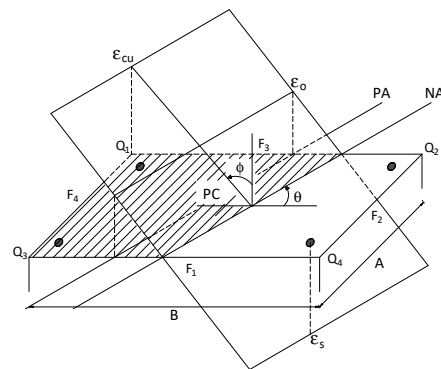


**Figure 2.** Strain distribution over a cross-section.

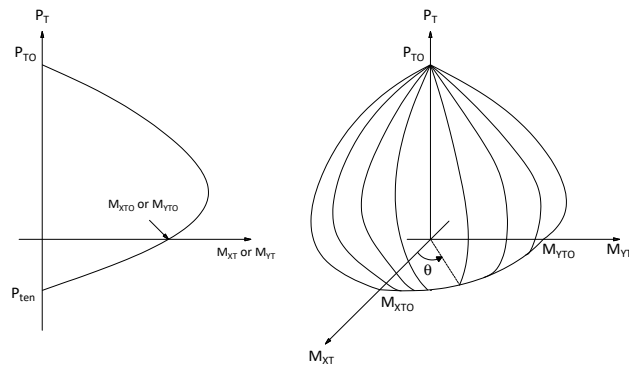


**Figure 3.** Typical interaction diagram (uniaxial bending) and failure surface (biaxial bending).

The compressive capacity ( $P_{TO}$ ) and tensile capacity ( $P_{ten}$ ) of the column, under concentric loading (where  $e = 0$ ), where the strain plane is parallel to the column's cross-sectional plane, define the extremities of the failure envelope. The intersection of the interaction diagram with the moment axis (horizontal axis) conceptually represents a condition of pure bending, leading to failure at theoretically infinite eccentricity. Here,  $M_{XTO}$  and  $M_{YTO}$  represent the moment capacities for such scenarios. Points within the interaction diagram or on the failure surface delineate a range of eccentricities limited by these critical values, indicating that failure is either dominated by axial loads at smaller eccentricities or by bending moments at larger eccentricities.

This flexural model of this study is founded on a critical assumption regarding the behavior of plane sections under bending stress. Specifically, it assumes that plane sections, which are planar prior to the application of flexure, maintain their planar geometry throughout the flexural deformation process. Consequently, the model prescribes a linear strain distribution across the section.

A crucial aspect of the model concerns the strain in the reinforcement, which is assumed to be consistent with the strain experienced by the adjacent concrete at their interface. This assumption implies a perfect bond condition between the concrete and the reinforcing bars, effectively eliminating any potential for debonding. Moreover, the model simplifies the representation of reinforcing bars as geometric points, assigning to each an area equivalent to that of the actual bar used. Despite their presence, the cross-sectional area occupied by the steel reinforcements is considered negligible and, thus, is not deducted from the concrete's total cross-sectional area.

An additional simplification inherent in this model is the complete disregard for the tensile strength of concrete. This assumption is predicated on the understanding that concrete's contribution to tensile resistance is minimal relative to its compressive capacity. The model identifies the onset of failure as the point at which any location within the section attains the maximum compressive strain defined for concrete.

It is important to note that the proposed model does not accommodate variations in the material behavior of concrete attributed to confinement effects. This limitation underscores a simplification in modeling the complex interactions within the concrete under varying stress states.

Throughout this investigation, a specific sign convention is employed for clarity and consistency in reporting results. According to this convention, compressive quantities are denoted as positive, while tensile quantities are represented as negative. This approach facilitates a straightforward interpretation of the model's outcomes.

In the analytical framework outlined in this study, the stress–strain relationships for concrete and steel reinforcement are essential in understanding and predicting the structural behavior under load. The model for concrete stress–strain (Figure 4a) follows the modified Hognestad curve [22–25], aligning with the recommendations made by Park and Paulay, 1975 [26]. This particular curve offers a refined approach to capturing the complex behavior of concrete under compression, emphasizing a more realistic representation of the material's response up to and including failure. For the steel reinforcement, the stress–strain relationship (Figure 4b) is characterized by an elastic–plastic model, again reflecting the guidelines proposed by Park and Paulay, 1975 [26]. This assumption permits a straightforward interpretation of the reinforcement's behavior, focusing on the transition from elastic performance to plastic deformation, a critical aspect in understanding the overall flexural behavior of reinforced concrete elements. It is important to acknowledge the flexibility of the model in terms of integrating alternative stress–strain curves. This adaptability underscores the model's potential applicability to a broad range of concrete and reinforcement materials, provided their stress–strain behaviors are well-documented and understood.

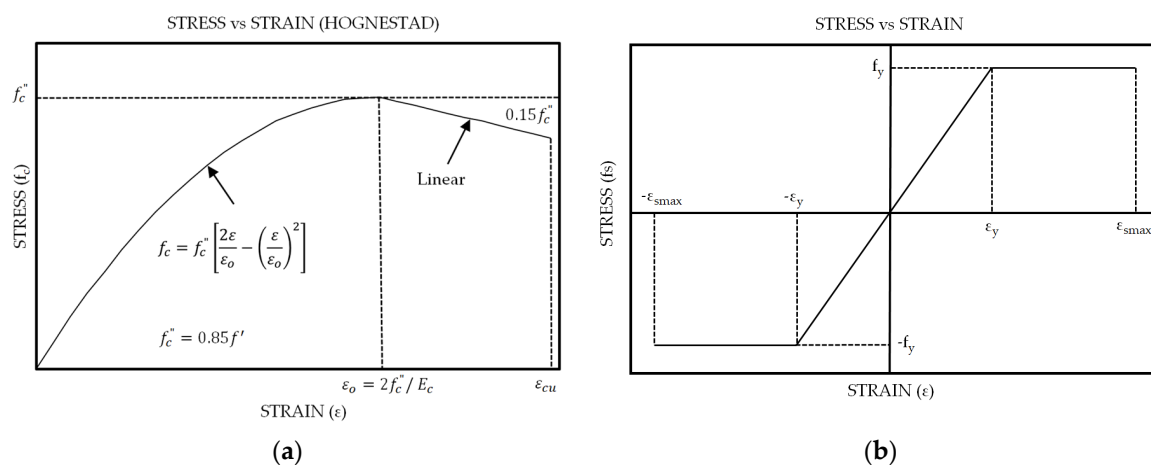


**Figure 4.** Cross-sectional material properties: (a) Stress vs. strain curve for concrete; (b) stress vs. strain curve for steel reinforcement.



Central to the proposed analytical model is the concept of failure, which is explicitly defined as the point at which concrete undergoes crushing at a strain level denoted as  $\varepsilon_{cu}$ . This definition implies that any strain distribution across a cross-section signifies a potential failure state if it includes at least one point where the concrete strain reaches  $\varepsilon_{cu}$ . This approach to defining failure is instrumental in constructing interaction diagrams, which graphically represent the relationship between axial forces and bending moments.

Determining a specific point on the interaction diagram involves analytical integration of the stresses corresponding to a given strain distribution. This calculation is critical in mapping out the failure envelope for the structure, providing insights into the limits of its load-bearing capacity. Bending moments, a key factor in this analysis, are calculated with respect to the plastic centroid of the section. This methodology facilitates a comprehensive understanding of the structural behavior, enabling the prediction of failure modes under various loading conditions.

Through this analytical framework (Figure 5), a robust tool for the assessment of reinforced concrete elements is aimed to be provided, offering insights that are crucial for both the design and analysis of such structures.

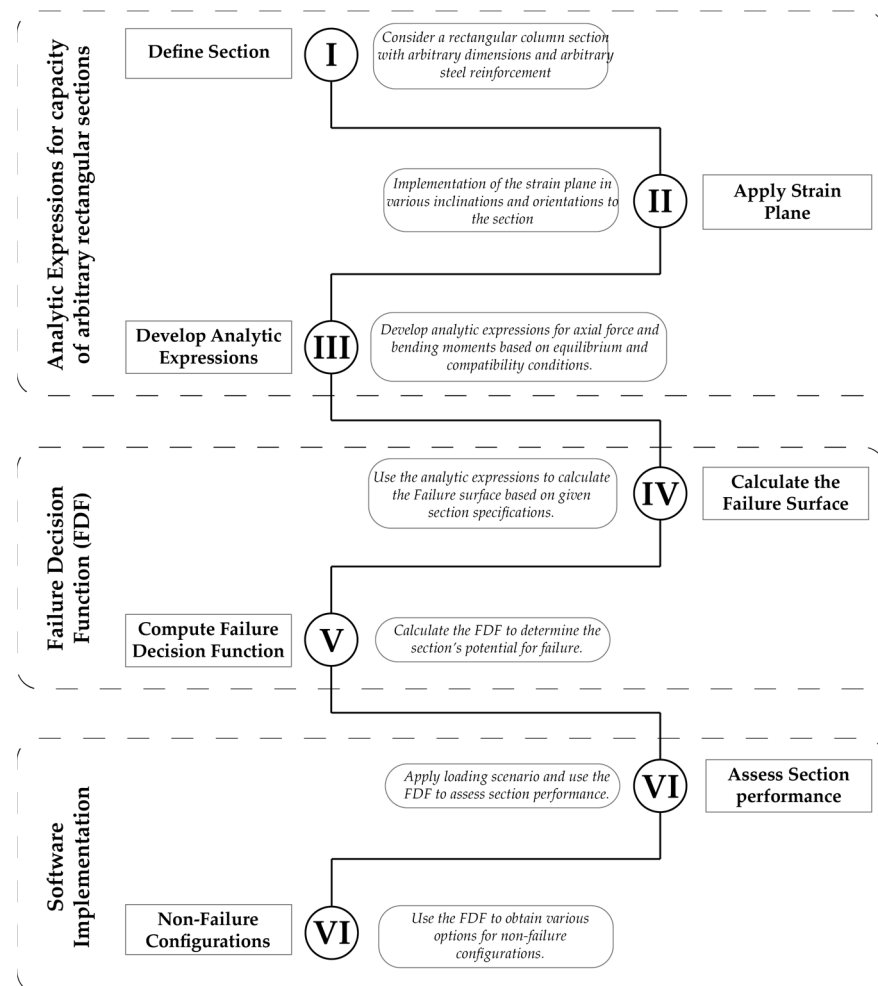


**Figure 5.** Flowchart of the proposed analytical framework.

A key contribution of this study is the formulation of analytic functions designed for determining precise points on the failure surface. These functions derive from the interplay between the geometry and material characteristics of rectangular sections, accommodating various patterns of steel reinforcement. Detailed in Supplementary S1 are the integral expressions for  $P_T$ ,  $M_{XT}$ , and  $M_{YT}$ , which outline the cross-sectional capacity. To facilitate

computation, this process is delineated into 14 distinct cases and sub-cases, as expounded in Supplementary S2.

Utilizing MATLAB software R2020b [27], these integrals are calculated, yielding analytic expressions that explicitly specify the axial force and bending moments across any possible strain distribution of the section, inclusive of all orientations of the neutral axis (NA). The expressions resulting from these calculations are cataloged in Supplementary S3. Remarkably, this means that a single set of expressions suffices for any rectangular column section and any combination of reinforcement. In essence, this framework requires only one comprehensive set of expressions to analyze all rectangular sections.

## 2.2. Generation of the Interaction Diagrams and Failure Surfaces

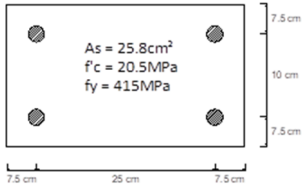
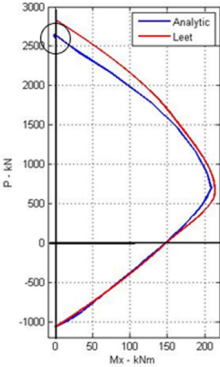
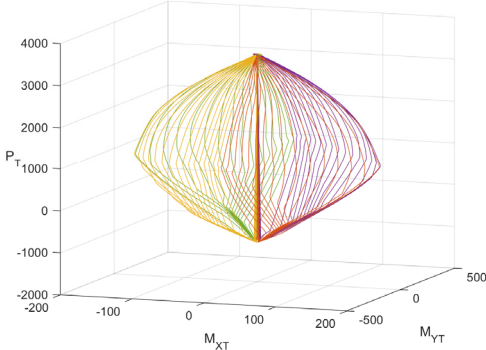
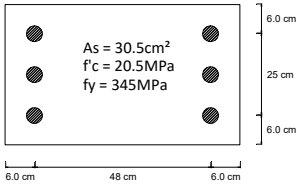
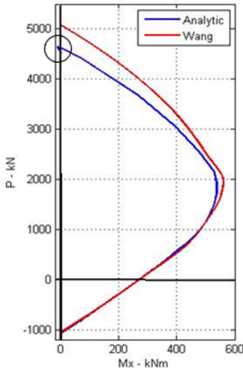
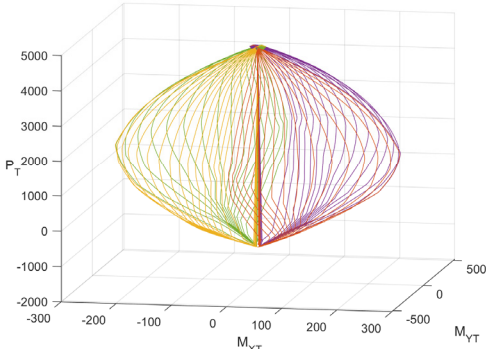
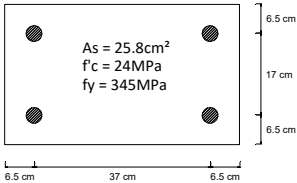
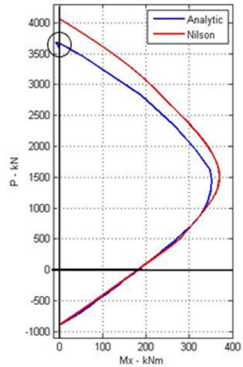
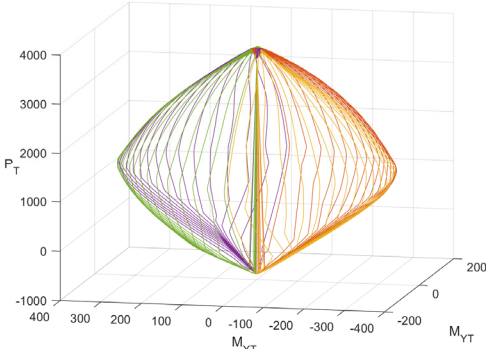
The analytic expressions are implemented in an algorithm coded in MATLAB to generate the array of points for all failure states (tension to compression) and plot the exact shape of the failure surface. The plot is based on a series of curves, each of which represents a failure state that corresponds to an orientation of the NA (defined by the angle  $\theta$ ). Each plot for  $\theta$  includes the points ( $P_T$ ,  $M_{XT}$ ,  $M_{YT}$ ) that correspond to any inclination of the strain plane (defined by the angle  $\varphi$ ), which has a strain equal to  $\varepsilon_{cu}$  at point Q1 and a strain value equal to  $\varepsilon_s$  at the extreme steel fiber (Figure 2). The inclinations of the strain plane are achieved by varying the strain values  $\varepsilon_s$  through the range  $\varepsilon_{smax} \leq \varepsilon < \varepsilon_{cu}$ , where  $\varepsilon_{smax}$  is the maximum tensile strain on the stress–strain curve for steel. The change of  $\varepsilon_s$  essentially defines a shift of the NA. This procedure is repeated for orientations of the NA ranging from  $0^\circ \leq \theta < 90^\circ$  to plot the failure surface in the first quadrant.

The process is repeated by changing successively the points from Q2 to Q4 and assigning the value of  $\varepsilon_{cu}$  at the respective locations (points Q2 to Q4). For any Q<sub>i</sub> the curve is generated in the respective quadrant of the failure surface. It is worth mentioning that if the reinforcement layout is symmetric, the values of axial force and bending moments in the quadrants are equal in magnitude but different in signs. As a result, for such cases, after the development of the failure surface in the first quadrant, the generation of the failure surface in the rest of the quadrants is trivial.

For the purpose of validating the effectiveness and accuracy of the proposed analytic method, its results have been benchmarked against established examples from the academic literature, as detailed in Table 1. Specifically, Section A compares the results with Example 7.7 from the work of Leet and Bernal, 1997, referenced as [28]. Section B engages with Example 13.14.1, as presented in the study by Wang and Salmon, 1979 [29]. Furthermore, Section C evaluates Example 8.1, derived from the research of Nilson and Winter, 1991 [3]. The comparison reveals that the outcomes of the analytic method closely align with those documented in the literature, underscoring its reliability and precision. Notably, certain discrepancies were observed across all cases, which are consistently accounted for and thoroughly examined in the subsequent discussion.

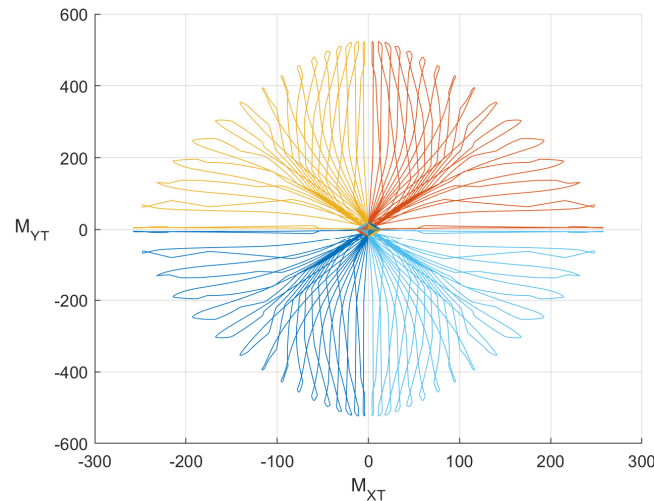
1. A lower value for the ultimate load,  $P_{TO}$  (Table 1), is calculated using the analytic method. The difference is attributed to the way of the calculation of the ultimate load. Based on examples found in the literature:  $P_{TO} = 0.85f'_c A_c + f_y A_s$  where  $A_c$  is the net area of concrete and  $A_s$  is the area of steel reinforcement. While this may be reasonable, it is not consistent with the assumptions regarding the failure of the section, which states that at least one point in the section must reach  $\varepsilon_{cu}$ . However, the stress in concrete is  $0.85f'_c$  at strain level  $\varepsilon_0$  and not at  $\varepsilon_{cu}$ . At strain level  $\varepsilon_{cu}$  the stress in concrete is  $0.85^2 f'_c = 0.7225 f'_c$  resulting in the smaller value of axial force calculated by the analytic method.
2. The curves for various orientations of the NA follow a pattern that is not of planar nature (Figure 6) as shown for typical interaction diagrams found in the literature. The non-planar shape explains why numerical methods sometimes cannot converge to particular points on the interaction diagram.

Table 1. Comparative Analysis of Verification Examples.

AA	Cross Section	Interaction Diagram	Failure Decision Function
A	<p>Example 7.7—Leet and Bernal (1997)</p> 		
B	<p>Example 13.14.1—Wang and Salmon (1979)</p> 		
C	<p>Example 8.1—Nilson and Winter (1991)</p> 		

3. The upper part of the interaction diagram or the failure surface calculated by the analytic method (Table 1) at strain levels just before the case of pure compression (i.e., when the strain on one side of the section equals to  $\epsilon_{cu}$  and on the other side is just below  $\epsilon_{cu}$  as shown in Figure 7 shows that the moments change sign/orientation. When the section is in pure compression, the strain distribution is uniform at the value  $\epsilon_{cu}$  and the bending moments become zero (assuming that the section is symmetric). Observing the stress–strain relation of concrete (Figure 4a), we note that prior to  $\epsilon_0$  as the value of the strain increases, so does the value of the stress. However, when the strains are greater than  $\epsilon_0$  then, as the value of the strain increases, the value of the stress decreases. As the strain plane tends to become horizontal (i.e., state of pure compression,  $\epsilon = \epsilon_{cu}$ ) then all points on the plane have values greater than

$\varepsilon_o$  (Figure 7). Based on the above, the stresses in the shaded area of the section are less than those in the non-shaded area. Considering that the area on both sides of the plastic centroid (shaded and non-shaded) are equal, then the resulting force on the shaded area is less than that of the non-shaded area, causing a moment with opposite sign.



**Figure 6.** Plan view of the failure surface (Example 13.14.1–Wang and Salmon (1979)).

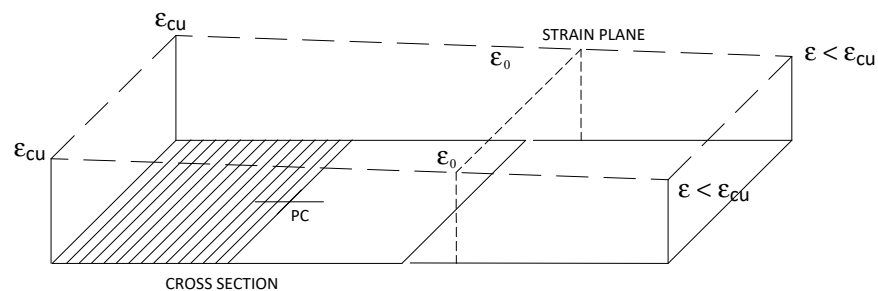


**Figure 7.** Strain plane orientation just before the section is in pure compression.

### 2.3. Failure Decision Function

The core objective of this research is to enhance the efficiency and accuracy of evaluating structural sections subjected to combined axial forces and bending moments. Central to this approach is the introduction of the Failure Decision Function (FDF), which simplifies the assessment process. The FDF is designed to quickly, accurately, and reliably determine the safety of a section under any combination of axial force and bending moments. This paper outlines the development process for the Failure Decision Function, detailing the steps necessary to achieve a tool that practitioners in the field can rely on for rapid and precise evaluations.

- Setup the model to develop the analytic functions for the computation of the exact shape of the failure surface (Section 2);
- Generate the failure surface for various types of cross-sections and reinforcement patterns using the analytic functions (Section 3);
- Develop a polynomial approximation for the failure surface by fitting a surface of the form  $F(P_T, M_{XT}, M_{YT}) = 0$  through the points of the actual curve. In this work, we utilized the MATLAB optimization toolbox coupled with an  $R^2$  test to ensure high accuracy. To ensure that the reduced set of points is well approximated by a smooth function, it is important to approximate each quadrant of angle  $\theta$ , of the failure surface separately. Basic reflection and reinforcement rearrangement operations enable the reduction of the approximation problem to fit in the first quadrant. Figure 8 shows a sample of the exact points (in blue) and points obtained by the best-fit polynomial

(in red). The  $R^2$  approximation index was computed at 0.97, which is considered satisfactory. The high accuracy of the approximation is also reflected in the Figure.

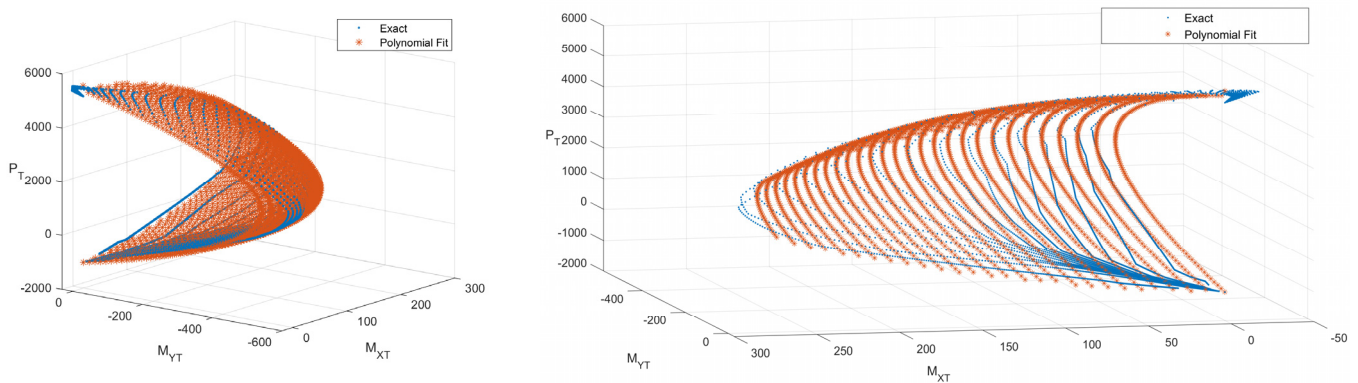


**Figure 8.** Three-dimensional visualization of the failure surface (in blue) and the corresponding Failure Decision Function (in orange).

- d. Define the Failure Decision Function. Considering that for a particular value of  $P_T$  there are multiple-moment couples ( $M_{XT}$ ,  $M_{YT}$ ) the failure surface in any quadrant cannot be expressed in the form of  $P_T = f(M_{XT}, M_{YT})$ . Rather, one can choose any of the two moments to be approximated as functions of the axial load and the other moment. The simplicity of polynomials, coupled with their significant approximation properties [30], has led the authors to select  $M_{YT} = f(P_T, M_{XT})$  as a polynomial function of  $P_T$  and  $M_{XT}$ . Numerical simulations indicate that the choice of moment on the right-hand side does not affect the quality of the approximation. The Failure Decision Function is defined as:

$$F(P_T, M_{XT}, M_{YT}) = f(P_T, M_{XT}) - M_{YT} \quad (1)$$

As shown in the next section, numerical simulations indicate that polynomials up to and including terms of degree three are sufficient for this problem. As a result, the Failure Decision Function in Equation (1) takes the form (2):

$$\begin{aligned} F(P_T, M_{XT}, M_{YT}) &= a_{00} + a_{10}P_T + a_{01}M_{XT} + a_{20}P_T^2 + a_{11}P_TM_{XT} + a_{02}M_{XT}^2 \\ &+ a_{30}P_T^3 + a_{21}P_T^2M_{XT} \\ &+ a_{12}P_TM_{XT}^2 + a_{03}M_{XT}^3 - M_{YT} \end{aligned} \quad (2)$$

The Failure Decision Function  $F(P_T, M_{XT}, M_{YT})$  can be used for a reliable and quick check of whether a section is safe or not subject to any combination of axial force and bending moments ( $P_T^*$ ,  $M_{XT}^*$ ,  $M_{YT}^*$ ). In detail, if  $F(P_T^*, M_{XT}^*, M_{YT}^*) < 0$ , the section is safe as the point is inside the failure surface, whereas if  $F(P_T^*, M_{XT}^*, M_{YT}^*) > 0$ , the section is not safe as the point is outside the failure surface.

Figure 9 provides an illustrative depiction of the Failure Decision Function (FDF) applied to evaluate the structural integrity of a fixed rectangular section—specifically, Section B, as outlined in Table 1—under various reinforcement scenarios. The Figure showcases four distinct reinforcement cases, each represented by different colors for clarity: purple, yellow (representing the two scenarios with lesser reinforcement), and orange, blue (depicting scenarios with greater reinforcement). A black circle illustrates a specific combination of axial load and bending moments applied to the section.



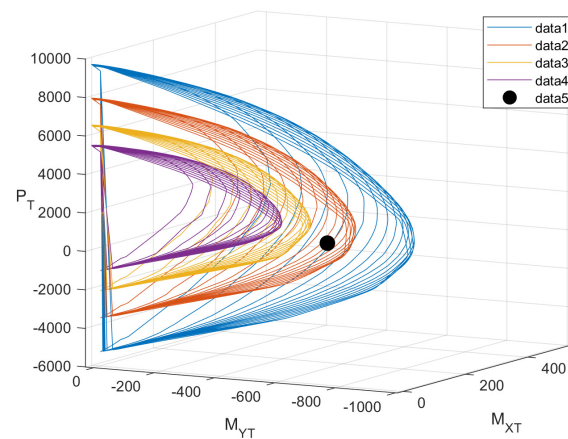


**Figure 9.** Representation of the Failure Decision Function for fixed rectangular RC concrete section with four distinct reinforcement options.

Analysis via the FDF reveals that the sections with lower levels of reinforcement (purple and yellow) are inadequate, as indicated by the black circle's position outside their respective curves. This external positioning signifies that the applied loads surpass the sections' failure thresholds, leading to a failure scenario. Conversely, for the sections with higher levels of reinforcement (orange and blue), the black circle falls within the safety bounds of their curves, indicating that these sections can safely withstand the applied load and moment combinations without failure. This graphical representation underscores the utility of the FDF in discerning between safe and unsafe structural configurations under specific loading conditions.

### 3. Results

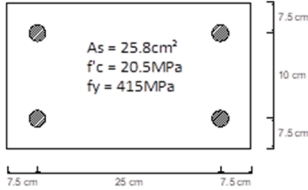
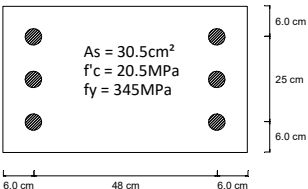
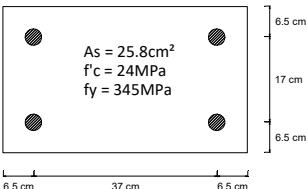
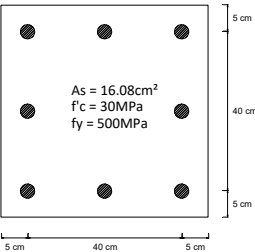
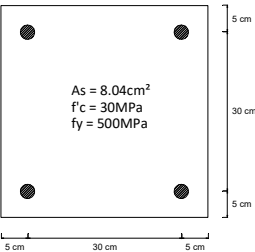
#### *Implications to Software*

The proposed analytical procedure introduces a simplified approach for efficiently computing the failure surface and the Failure Decision Function (FDF) across a broad spectrum of cross-sectional shapes and material properties. This innovative method promises to significantly reduce the time and effort traditionally required for such analyses, presenting a one-time computation process that yields extensive utility for various engineering applications. Following the initial determination of the failure surface and FDF, this methodology facilitates its integration into structural engineering software, enhancing the capabilities of such applications in two significant aspects:

- a. Compile a library of *Failure Decision Functions*, similar to Table 2, in software applications and perform capacity checks without the requirement of developing the failure surfaces, thus saving computational time. Further, include a feature that will enable the software to “suggest” safe cross sections and reinforcement combinations for the applied  $(P_T^*, M_{XT}^*, M_{YT}^*)$ . The latter will provide the user with the flexibility to experiment with dimensions and reinforcement options prior to running the analysis again.



Table 2. Sample Failure Decision Functions.

AA		Section	Failure Decision Function $F(P_T, M_{XT}, M_{YT}) = a_{00} + a_{10}P_T + a_{01}M_{XT} + a_{20}P_T^2 + a_{11}P_TM_{XT} + a_{02}M_{XT}^2 + a_{30}P_T^3 + a_{21}P_T^2M_{XT} + a_{12}P_TM_{XT}^2 + a_{03}M_{XT}^3 - M_{YT}$
A	Example 7.7—Leet and Bernal (1997)		$a_{00} = -146.9,$ $a_{10} = -0.08211,$ $a_{01} = -0.1805,$ $a_{20} = 0.00005179,$ $a_{11} = -0.000390,$ $a_{02} = 0.03124,$ $a_{30} = 5 \times 10^{-10},$ $a_{21} = 3.779 \times 10^{-7},$ $a_{12} = 1.07 \times 10^{-6},$ $a_{03} = -0.00003449.$
			$a_{00} = -283,$ $a_{10} = -0.2076,$ $a_{01} = -0.5732,$ $a_{20} = 0.00005867,$ $a_{11} = -0.0007491,$ $a_{02} = 0.01511,$ $a_{30} = 1.662 \times 10^{-11},$ $a_{21} = 2.033 \times 10^{-7},$ $a_{12} = 3.524 \times 10^{-7},$ $a_{03} = -0.00001534.$
B	Example 13.14.1—Wang and Salmon (1979)		$a_{00} = -192.8,$ $a_{10} = -0.1621,$ $a_{01} = -0.5575,$ $a_{20} = 0.00006145,$ $a_{11} = -0.0009175,$ $a_{02} = 0.02398,$ $a_{30} = -6.702 \times 10^{-10},$ $a_{21} = 3.128 \times 10^{-7},$ $a_{12} = 7.435 \times 10^{-7},$ $a_{03} = -0.0000473.$
			$a_{00} = -205.1,$ $a_{10} = -0.1815,$ $a_{01} = -0.2328,$ $a_{20} = 0.00004419,$ $a_{11} = -0.0005301,$ $a_{02} = 0.005983,$ $a_{30} = -1.827 \times 10^{-9},$ $a_{21} = 7.375 \times 10^{-8},$ $a_{12} = 1.643 \times 10^{-7},$ $a_{03} = -4.974 \times 10^{-6}.$
C	Example 8.1—Nilson and Winter (1991)		$a_{00} = -76.65,$ $a_{10} = -0.1645,$ $a_{01} = -0.2259,$ $a_{20} = 0.00006181,$ $a_{11} = -0.00105,$ $a_{02} = 0.01347,$ $a_{30} = -4.14 \times 10^{-9},$ $a_{21} = 2.302 \times 10^{-7},$ $a_{12} = 6.157 \times 10^{-7},$ $a_{03} = -0.00002373.$
			$a_{00} = -76.65,$ $a_{10} = -0.1645,$ $a_{01} = -0.2259,$ $a_{20} = 0.00006181,$ $a_{11} = -0.00105,$ $a_{02} = 0.01347,$ $a_{30} = -4.14 \times 10^{-9},$ $a_{21} = 2.302 \times 10^{-7},$ $a_{12} = 6.157 \times 10^{-7},$ $a_{03} = -0.00002373.$
D	Section 50 cm × 50 cm		$a_{00} = -76.65,$ $a_{10} = -0.1645,$ $a_{01} = -0.2259,$ $a_{20} = 0.00006181,$ $a_{11} = -0.00105,$ $a_{02} = 0.01347,$ $a_{30} = -4.14 \times 10^{-9},$ $a_{21} = 2.302 \times 10^{-7},$ $a_{12} = 6.157 \times 10^{-7},$ $a_{03} = -0.00002373.$
			$a_{00} = -76.65,$ $a_{10} = -0.1645,$ $a_{01} = -0.2259,$ $a_{20} = 0.00006181,$ $a_{11} = -0.00105,$ $a_{02} = 0.01347,$ $a_{30} = -4.14 \times 10^{-9},$ $a_{21} = 2.302 \times 10^{-7},$ $a_{12} = 6.157 \times 10^{-7},$ $a_{03} = -0.00002373.$
E	Section 40 cm × 40 cm		$a_{00} = -76.65,$ $a_{10} = -0.1645,$ $a_{01} = -0.2259,$ $a_{20} = 0.00006181,$ $a_{11} = -0.00105,$ $a_{02} = 0.01347,$ $a_{30} = -4.14 \times 10^{-9},$ $a_{21} = 2.302 \times 10^{-7},$ $a_{12} = 6.157 \times 10^{-7},$ $a_{03} = -0.00002373.$
			$a_{00} = -76.65,$ $a_{10} = -0.1645,$ $a_{01} = -0.2259,$ $a_{20} = 0.00006181,$ $a_{11} = -0.00105,$ $a_{02} = 0.01347,$ $a_{30} = -4.14 \times 10^{-9},$ $a_{21} = 2.302 \times 10^{-7},$ $a_{12} = 6.157 \times 10^{-7},$ $a_{03} = -0.00002373.$

As a practical demonstration of the methodology's applicability, Table 3 lists an extract of 24 test scenarios from a dataset encompassing 123 distinct test scenarios, each

characterized by unique configurations of concrete dimensions and steel reinforcement layouts. Additionally, the table documents the outcomes generated by the Failure Decision Function (FDF) when applied to a specific set of loading conditions. The function is evaluated for the loading scenario  $(P_T^*, M_{XT}^*, M_{YT}^*) = (300, 150, -200)$ , which represents a particular combination of axial force and bending moments. These data not only validate the FDF's efficacy across a diverse range of structural scenarios but also demonstrate its potential for reliable, real-time analysis in structural engineering applications. In the proposed software application, users input a loading scenario consisting of an axial load and biaxial moments  $(P_T^*, M_{XT}^*, M_{YT}^*)$ , along with the proposed cross-sectional dimensions, number of steel bars, bar diameter, and location of each steel bar. The application provides real-time feedback indicating whether the selected combination is likely to fail. In the event of a failure, users can modify the dimensions or adjust the steel reinforcement to explore alternative configurations that meet the non-failure criteria. In addition, the application enables users to explore various options of non-failure configurations.

**Table 3.** Test cases with the implementation of the Failure Decision Function (Bar Diam. = 16 mm (Y16),  $n_x$  = # of bars in x direction,  $n_y$  = # of bars in y direction, A, B = Cross Section Dimensions).

A	$n_y$	B	$n_x$	FDF	A	$n_y$	B	$n_x$	FDF
0.3	2	0.5	5	F	0.4	2	0.6	2	F
0.3	3	0.5	5	F	0.5	5	0.4	4	P
0.3	2	0.6	2	F	0.4	3	0.6	2	F
0.3	3	0.6	2	F	0.4	4	0.6	2	F
0.3	2	0.6	3	F	0.4	2	0.6	3	F
0.4	4	0.5	3	F	0.4	3	0.6	3	F
0.4	2	0.5	4	F	0.4	4	0.6	3	P
0.4	3	0.5	4	F	0.4	2	0.6	4	F
0.4	4	0.5	4	P	0.4	3	0.6	4	P
0.4	2	0.5	5	F	0.4	4	0.6	4	P
0.4	3	0.5	5	P	0.5	2	0.5	2	F
0.4	4	0.5	5	P	0.5	3	0.5	2	F

In each of the 123 test cases, the authors precisely computed the failure surface points utilizing analytic formulas, subsequently constructed the Failure Decision Function, and applied it to assess the specific axial load and moment combination  $(P_T^*, M_{XT}^*, M_{YT}^*) = (300, 150, -200)$ . These computations were efficiently performed in just fifteen (15) seconds on an i7 processor equipped with 12 GB of RAM. This performance highlights the method's efficiency, demonstrating that the failure check for a load–moment combination relative to a single section can be executed almost instantaneously.

- b. Develop an application that dynamically generates the Failure Decision Function for any specified set of cross-sectional geometries, material properties, and reinforcement patterns. This tool will allow users to “experiment” with different combinations of axial loads and bending moments to evaluate the structural suitability of various sections. The capability to provide instantaneous assessments makes this application particularly valuable in several key engineering activities:
  - i. Preliminary Design Stage: The application can be utilized to generate trial sections during the initial design phase, enabling designers to quickly iterate over different section configurations. By assessing various combinations of loads and moments, engineers can optimize structural elements efficiently, ensuring that the preliminary designs meet all necessary safety and performance criteria;
  - ii. Site Inspection: During construction or routine inspections, especially in instances where there are deviations from the initial designs, the application serves as a critical tool for on-the-spot assessments of section capacity. This functionality is crucial for verifying the structural integrity of sections when

unexpected changes or errors are detected in the construction phase, thereby aiding in immediate decision-making to address potential safety concerns.

The real-time operation of this application not only enhances the flexibility and efficiency of structural design and verification processes but also supports the adaptive assessment capabilities required in dynamic construction environments.

#### 4. Discussion

The novelty of the approach that is presented in this study relies on the fact that the capacity assessment of the section for any loading scenario is provided through the Failure Decision Function (FDF). The main outcomes of the study are listed below:

- Analytic method for constructing uniaxial interaction diagrams and biaxial bending failure surfaces for rectangular reinforced concrete sections. This method utilizes the nonlinear stress–strain relationships for concrete and steel reinforcement to develop precise mathematical expressions;
- Analytic formulae developed within this paper enable the rapid computation of the FDF;
- Failure Decision Function (FDF) is a tool designed to assess the structural integrity of columns subjected to axial forces and either uniaxial or biaxial bending moments.

A major contribution of this research is the detailed characterization of the geometry of the failure surface. It has been revealed that the curves, which depend on the orientation (angle  $\theta$ ) of the neutral axis, are not planar. Particularly at higher parts of these curves, near the pure compression strain levels, the moments exhibit changes in sign or orientation. This insight adds significant depth to the existing literature on structural failure analysis.

Additionally, the computation of the maximum axial force, derived from the analytic method at the critical strain level ( $\epsilon_{cu}$ ), aligns with established failure assumptions but presents a lower force value than traditionally cited in the literature, which typically uses a different baseline strain ( $\epsilon_o$ ). This finding suggests that a potential recalibration of standard practices might be warranted to enhance the accuracy and safety of structural assessments.

#### 5. Conclusions

This study introduces an approach for assessing rectangular reinforced concrete columns using the Failure Decision Function (FDF). It develops an analytic method for constructing uniaxial interaction diagrams and biaxial bending failure surfaces by utilizing nonlinear stress–strain relationships and section properties, enabling mathematical expressions for axial force and bending moments. This method enhances the safety and accuracy of capacity failure representation in the design of rectangular reinforced concrete columns. The FDF facilitates real-time testing of various section dimensions and reinforcement configurations. When integrated into software, this capability streamlines design and evaluation processes, making them efficient and responsive. Additionally, the FDF can be incorporated into software libraries for immediate assessment of structural integrity under axial forces and bending moments, further improving the efficiency and responsiveness of structural analysis software. The study's detailed characterization of the failure surface reveals non-planar curves dependent on the neutral axis orientation, enhancing the understanding of structural failure of rectangular reinforced concrete columns. In conclusion, the findings advance the efficiency of structural design and assessment for reinforced concrete columns, simplifying structural assessments.

**Supplementary Materials:** The following supporting information can be downloaded at: <https://www.mdpi.com/article/10.3390/inventions9030063/s1>.

**Author Contributions:** Conceptualization, P.C.; methodology, P.C. and M.C.; software, M.C.; validation, P.C., M.C. and D.N.; formal analysis, P.C. and M.C.; investigation, P.C. and M.C.; data curation, G.X.; writing—original draft preparation, P.C. and M.C.; writing—review and editing, D.N. and G.X.; supervision, P.C. All authors have read and agreed to the published version of the manuscript.

**Funding:** This research received no external funding.

**Data Availability Statement:** All data supporting results can be found in the Supplementary Materials.

**Conflicts of Interest:** The authors declare no conflicts of interest.

## References

- Grasser, E.; Linse, D. *Bemessungstabellen für Stahlbetonquerschnitte Auf der Grundlage der Neuen DIN 1045*; Werner Verlag: Düsseldorf, Germany, 1972.
- Duțulescu, E. Näherungsverfahren bei zweiachsiger Biegung mit Normalkraft. *Beton-Stahlbetonbau* **2015**, *110*, 254–269. [\[CrossRef\]](#)
- Nilson, A.H.; Winter, G. *Design of Concrete Structures*, 11th ed.; McGraw-Hill Inc.: New York, NY, USA, 1991. Available online: <https://www.amazon.co.uk/Design-Concrete-Structures-Arthur-Nilson/dp/0070465673> (accessed on 23 May 2024).
- Papanikolaou, V.K.; Sextos, A.G. Design charts for rectangular R/C columns under biaxial bending: A historical review toward a Eurocode-2 compliant update. *Eng. Struct.* **2016**, *115*, 196–206. [\[CrossRef\]](#)
- Kolapkar, B.N.; Balakrishnan, B.; Menon, D. Biaxial bending of RC rectangular column sections: Improved ‘load contour’ formulation. *Struct. Concr.* **2023**. [\[CrossRef\]](#)
- Dundar, C.; Tokgoz, S.; Tanrikulu, A.K.; Baran, T. Behaviour of reinforced and concrete-encased composite columns subjected to biaxial bending and axial load. *Build. Environ.* **2008**, *43*, 1109–1120. [\[CrossRef\]](#)
- Pallarés, L.; Bonet, J.L.; Miguel, P.F.; Fernández Prada, M.A. Experimental research on high strength concrete slender columns subjected to compression and biaxial bending forces. *Eng. Struct.* **2008**, *30*, 1879–1894. [\[CrossRef\]](#)
- Fafitis, A. Interaction Surfaces of Reinforced Concrete Sections in Biaxial Bending by Green’s Theorem. In Proceedings of the 8th International Conference on Computing in Civil and Building, Stanford, CA, USA, 14–16 August 2000. [\[CrossRef\]](#)
- Papanikolaou, V.K. Analysis of arbitrary composite sections in biaxial bending and axial load. *Comput. Struct.* **2012**, *98–99*, 33–54. [\[CrossRef\]](#)
- Matuszak, A.; Pluciński, P. *Accuracy of Cross-Section Stress Numerical Integration by Boundary Integration Formulae*; CRC Press eBooks: Boca Raton, FL, USA, 2014; pp. 111–120. [\[CrossRef\]](#)
- Lejano, B. Investigation of Biaxial Bending of Reinforced Concrete Columns through Fiber Method Modeling. Available online: [https://www.sefindia.org/forum/files/column\\_126.pdf](https://www.sefindia.org/forum/files/column_126.pdf) (accessed on 10 April 2024).
- Christou, P.; Michael, A.; Anastasiou, C.; Nicolaides, D. Effect of confinement on the interaction diagrams for rc sections with cfrp grids and wraps. *Int. J. Comput. Methods Exp. Meas. (Print)* **2013**, *1*, 265–282. [\[CrossRef\]](#)
- Kwak, H.-G.; Kwak, J.-H. An improved design formula for a biaxially loaded slender RC column. *Eng. Struct.* **2010**, *32*, 226–237. [\[CrossRef\]](#)
- Bouazid, T.; Demagh, K. Practical method for analysis and design of slender reinforced concrete columns subjected to biaxial bending and axial loads. *Slovak J. Civ. Eng.* **2011**, *XIX*, 24–32. [\[CrossRef\]](#)
- Di Laora, R.; Galasso, C.; Mylonakis, G.; Cosenza, E. A simple method for N-M interaction diagrams of circular reinforced concrete cross sections. *Struct. Concr.* **2019**, *21*, 48–55. [\[CrossRef\]](#)
- Rodriguez, J.A.; Aristizabal-Ochoa, J.D. Biaxial Interaction Diagrams for Short RC Columns of Any Cross Section. *J. Struct. Eng.* **1999**, *125*, 672–683. [\[CrossRef\]](#)
- Quaranta, G.; Trentadue, F.; Marano, G.C. Closed-form approximation of the axial force-bending moment interaction diagram for hollow circular reinforced concrete cross-sections. *Eng. Struct.* **2017**, *153*, 516–524. [\[CrossRef\]](#)
- Vaz Rodrigues, R. A new technique for ultimate limit state design of arbitrary shape RC sections under biaxial bending. *Eng. Struct.* **2015**, *104*, 1–17. [\[CrossRef\]](#)
- Shustin, P.F.; Avron, H. Gauss-Legendre Features for Gaussian Process Regression. *arXiv* **2021**, arXiv:2101.01137. [\[CrossRef\]](#)
- da Silva, V.D.; Barros, M.H.F.M.; Julio, E.N.B.S.; Ferreira, C.C. Closed form ultimate strength of multi-rectangle reinforced concrete sections under axial load and biaxial bending. *Comput. Concr.* **2009**, *6*, 505–521. [\[CrossRef\]](#)
- Schneider, P.; Eberly, D.H. *Geometric Tools for Computer Graphics*; Elsevier: Amsterdam, The Netherlands, 2002.
- Panjehpour, M.; Chai, H.K.; Voo, Y.L. Refinement of Strut-and-Tie Model for Reinforced Concrete Deep Beams. *PLoS ONE* **2015**, *10*, e0130734. [\[CrossRef\]](#) [\[PubMed\]](#)
- Numerical and Analytical Modeling of Concrete Confined with FRP Wraps. Available online: [https://etda.libraries.psu.edu/files/final\\_submissions/10784](https://etda.libraries.psu.edu/files/final_submissions/10784) (accessed on 12 April 2024).
- Michael, A.; Hamilton, H.R. Experimental ductility of compression-controlled flexural members using CFRP grid to confine concrete. *Materials* **2021**, *14*, 5163. [\[CrossRef\]](#) [\[PubMed\]](#)
- Oztekin, E.; Pul, S.; Husem, M. Determination of rectangular stress block parameters for high performance concrete. *Eng. Struct.* **2003**, *25*, 371–376. [\[CrossRef\]](#)
- Park, R.; Paulay, T. Ultimate Deformation and Ductility of Members with Flexure. In *Reinforced Concrete Structures*; John Wiley & Sons: Hoboken, NJ, USA, 1975; pp. 195–269. [\[CrossRef\]](#)
- MathWorks MATLAB—MathWorks. Mathworks.com. 2019. Available online: <https://www.mathworks.com/products/matlab.html> (accessed on 10 April 2024).
- Leet, K.; Bernal, D. *Reinforced Concrete Design*; McGraw-Hill Companies: New York, NY, USA, 1997.

29. Wang, C.K.; Salmon, C.G. Reinforced Concrete Design. trid.trb.org. 1979. Available online: <https://trid.trb.org/view/502701> (accessed on 23 May 2024).
30. Heiberger, R.M.; Neuwirth, E. Polynomial Regression. In *R through Excel*; Springer: New York, NY, USA, 2009; pp. 269–284. [[CrossRef](#)]

**Disclaimer/Publisher’s Note:** The statements, opinions and data contained in all publications are solely those of the individual author(s) and contributor(s) and not of MDPI and/or the editor(s). MDPI and/or the editor(s) disclaim responsibility for any injury to people or property resulting from any ideas, methods, instructions or products referred to in the content.